

Unraveling the exciton binding energy and the dielectric constant in single crystal methylammonium lead tri-iodide perovskite

Zhuo Yang,^{1,*} Alessandro Surrente,^{1,*} Krzysztof Galkowski,¹ Nicolas Bruyant,¹ Duncan K. Maude,¹ Amir Abbas Haghighirad,² Henry J. Snaith,² Paulina Plochocka,^{1,†} and Robin J. Nicholas^{2,‡}

¹*Laboratoire National des Champs Magnétiques Intenses,
UPR 3228, CNRS-UGA-UPS-INSA, Grenoble and Toulouse, France*

²*University of Oxford, Clarendon Laboratory, Parks Road, Oxford, OX1 3PU, United Kingdom*
(Dated: January 19, 2017)

We have accurately determined the exciton binding energy and reduced mass of single crystals of methylammonium lead tri-iodide using magneto-reflectivity at very high magnetic fields. The single crystal has excellent optical properties with a narrow line width of ~ 3 meV for the excitonic transitions and a 2s transition which is clearly visible even at zero magnetic field. The exciton binding energy of 16 ± 2 meV in the low temperature orthorhombic phase is almost identical to the value found in polycrystalline samples, crucially ruling out any possibility that the exciton binding energy depends on the grain size. In the room temperature tetragonal phase, an upper limit for the exciton binding energy of 12 ± 4 meV is estimated from the evolution of 1s-2s splitting at high magnetic field.

Solar cells based on hybrid organic-inorganic perovskites have demonstrated an exceptionally rapid increase in the photovoltaic energy conversion efficiency, which has recently reached record values of more than 20%.^{1–4} These materials crystallize in the form ABX_3 , where A is an organic ammonium cation (typically methylammonium, MA, or formamidinium, FA), B is Pb or Sn and X is a halide, with methylammonium lead tri-iodide ($MAPbI_3$) being arguably the most studied compound. Their success as light harvesters in solar cells is due to the combined effect of their excellent absorption properties,⁵ a large carrier diffusion length^{6,7} and easy fabrication.^{8,9} This striking success has generated research on a wide variety of perovskite based photonic devices, including light emitting diodes,¹⁰ lasers,¹¹ photodetectors,¹² and single photon sources.¹³

A question currently under debate, important both from a fundamental point of view and for the optimization of perovskite based devices, is the value of the exciton binding energy. Early magneto-optical studies,^{5,14,15} together with absorption measurements,¹⁶ suggested an exciton binding energy $\simeq 40 - 50$ meV for $MAPbI_3$. This would imply that a significant fraction of photogenerated carriers form excitonic bound states at room temperature, with important consequences for the architecture of solar cells. However, when the frequency dependence of the dielectric constant^{17,18} is taken into account, the estimated exciton binding energies are in the range 2 – 15 meV.^{17–21} It has been suggested that discrepancies in the exciton binding energy might be due to the grain size and to the environment surrounding the grains.¹⁶ Polycrystalline perovskites have a large density of defects at the surface and at grain boundaries,²² which influence the carrier mobility and diffusion length, with an increased diffusion length in films with enhanced grain size.²³

The recent synthesis of single crystal perovskites has allowed the trap density to be reduced significantly, lead-

ing to a dramatically enhanced diffusion length and carrier mobility.^{24–26} The optical characterization of a single crystal methylammonium lead tri-bromide suggests that the exciton binding energy is $\simeq 15$ meV²⁷ at low temperature, however, in the absence of magnetic field, the exciton binding energy could not be determined in the technologically important cubic crystal phase at room temperature. A low exciton binding energy supports the free carrier scenario at room temperature, consistent with the photoluminescence of single crystal $MAPbI_3$ at 300 K.²⁸

In this paper, we report on the first interband magneto-optical studies of a single crystal hybrid organic-inorganic perovskite, $MAPbI_3$, enabling the direct measurement of the exciton binding energy and reduced mass in both the orthorhombic and tetragonal phases. Magneto reflectivity measurements are analyzed for the first time and allow us to accurately determine these quantities without knowing the dielectric constant. The values obtained are identical to those measured in polycrystalline thin films using magneto-absorption,²⁹ unequivocally demonstrating that the exciton binding energy does not depend on the grain size.

Single crystals of $MAPbI_3$ were grown from seed crystals in supersaturated solution and oriented by Laue diffraction. The magnetorefectivity measurements were performed in pulsed magnetic fields up to 66 T, with a typical pulse duration of ~ 300 ms. The sample was placed in a liquid helium cryostat and immersed in liquid or gaseous helium. White light, provided by a broadband halogen lamp, was coupled to a multimode fiber. The reflected signal was collected by a fiber bundle in the Faraday configuration with the light wavevector parallel to the applied magnetic field. A monochromator coupled to a liquid nitrogen cooled CCD camera was used to analyze the reflected signal. Typical exposure time was 2 ms, which allows spectra to be measured at essentially constant magnetic field.

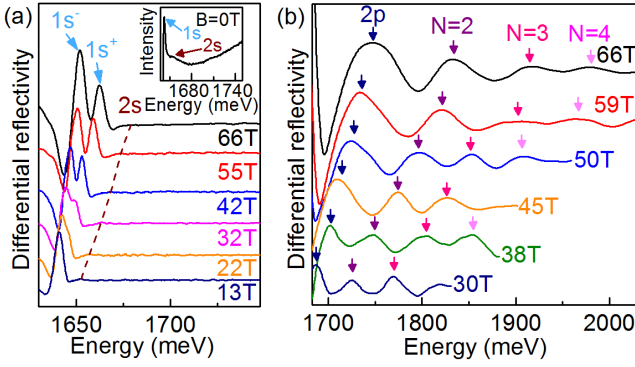


FIG. 1. (color online) (a) Reflectivity spectra measured at the indicated magnetic field values. The spectra are vertically offset for clarity. The arrows mark the relevant absorption peaks. Inset: as-measured reflectivity spectrum at zero magnetic field. (b) High magnetic field differential reflectivity spectra after normalization by zero field reflectivity. Arrows of the same colours indicate the transition between the same Landau levels.

The reflectivity data was fitted using the relation

$$R(E) = R_0 + \sum_j A_j \operatorname{Re} \left(\frac{E_j - E + i\gamma_j}{\gamma_j^2 + (E - E_j)^2} \right) \quad (1)$$

where A_j , E_j and γ_j are the amplitude, energy and broadening parameter for each of the resonances present.³⁰ R_0 is a constant (background) which controls the total amplitude of the reflectivity signal. In practice taking the negative derivative of the fitted reflectivity with respect to energy, $(-dR/dE)$, produces peaks at almost exactly the energies of the resonant absorption, as expected from a Kramers-Kronig analysis. The data were therefore analyzed and could be more easily displayed by taking the negative derivative of the measured reflectivity.

Representative differential magneto reflectivity spectra measured at 2 K are shown in Fig. 1 for magnetic fields up to 66 T. In Fig. 1(a) we show the spectral region where the strongest excitonic features are visible. At low magnetic field, the pronounced peak corresponds to the absorption of the 1s exciton state at an energy of 1640 meV. The single crystal MAPbI₃ has excellent crystalline quality, with for the 1s transition a fitted broadening parameter of 3.8 meV, compared with typical values of $\gtrsim 20$ meV for polycrystalline thin films.²⁹ The narrow linewidth of the 1s transition enables us to resolve an additional weak absorption peak on the high energy side of the 1s peak, attributed to the 2s excitonic state, visible here even at zero magnetic field. This is highlighted in the inset of Fig. 1(a), where we show the raw reflectivity spectrum at zero magnetic field $R(B=0)$.

Previously, in thin film MAPbI₃, the 2s state was only observed as a weak shoulder at high magnetic fields,²⁹ while the large broadening of the 1s transition of Br-based MA perovskites precluded the observation of the 2s

state even at high magnetic field.³¹ The small linewidth of the 1s state also allows the observation of the Zeeman splitting of the 1s transition without the need for polarizing optics in the detection path (the splitting is clearly seen in Fig. 1(a) for $B \geq 45$ T). By extracting the energies of the Zeeman-split 1s states from magneto-reflectivity measurements, we obtained a linear splitting yielding $g_{\text{eff}} = 2.66 \pm 0.1$. This value is slightly larger than previously reported,⁵ possibly due to the improved resolution of our measurements, but nevertheless similar to our previous results obtained on thin films.³¹ Finally, the high-energy absorption peaks can be better seen by plotting the spectra obtained by differentiating the spectrum normalized by the spectrum measured at zero field. These spectra are shown in Fig. 1(b), where a series of maxima, identified with the resonant absorption involving interband transitions between Landau levels, can be seen.

The observation of two hydrogenic bound states accompanied by inter Landau level transitions gives a very well defined measurement of some of the fundamental parameters for bulk MAPbI₃ such as the exciton binding energy and the reduced mass which have proved to be highly controversial.^{5,14,15,17–20,29,31} The measurements of these two parameters are effectively decoupled, as they influence the observed transition energies in distinctly different regions of the energy spectrum. The energy $E_{n,0}(\gamma)$ of the hydrogen-like neutral exciton transitions close to the band edge can be described using a numerical solution of the hydrogen atom in strong magnetic field.³² The transition energy depends on the dimensionless parameter $\gamma = \hbar\omega_c/2R^*$, where $\omega_c = eB/\mu$ is the cyclotron frequency, and μ is the reduced effective mass of the exciton, defined as $\mu^{-1} = m_e^{-1} + m_h^{-1}$, where m_e and m_h denote the effective mass of the electron and hole.

The Zeeman splitting of the excitonic transitions seen in Fig. 1(a) is included by introducing a Zeeman splitting term in the hydrogen-like absorption spectrum³¹. Additionally, the higher energy transitions, at high magnetic field where $\gamma > 1$, approach the free carrier interband transition between Landau levels,³³ with energies given by

$$E(B) = E_g + \left(n + \frac{1}{2}\right) \hbar\omega_c \pm \frac{1}{2} g_{\text{eff}} \mu_B B,$$

where E_g is the band gap, $n = 0, 1, 2, \dots$ represents the Landau orbital quantum number in the valence and conduction bands, g_{eff} is the effective g -factor for the Zeeman splitting and μ_B designates the Bohr magneton.

In Fig. 2, we show the full set of observed transitions. For the higher energy dipole allowed ($\Delta n = 0$) interband Landau level transitions, the dominant fitting parameter is the reduced effective mass of the exciton, which is determined to be $\mu = (0.104 \pm 0.005)m_0$, where m_0 is the free electron mass, consistent with the theoretically calculated values from density functional theory of $\mu = 0.099m_0 - 0.11m_0$,^{34,35} and in excellent agreement with the experimentally determined effective mass

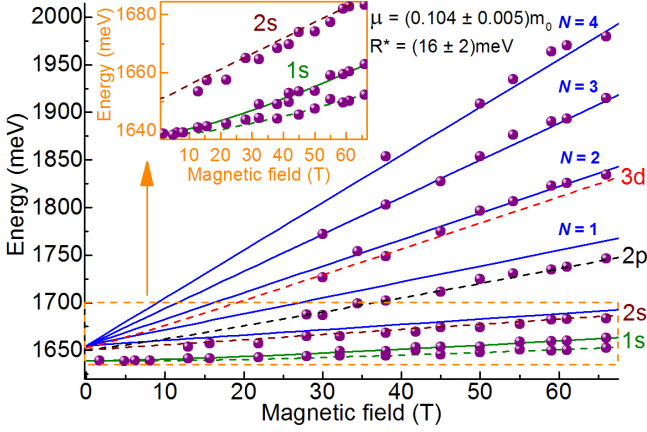


FIG. 2. (color online) Energies for excitonic and Landau level transitions as a function of the applied magnetic field. Blue, solid lines are the results of linear fits of the interband transition between Landau levels in the valence and conduction bands. Dashed lines result from the fit of hydrogen-like transitions. Inset: close-up view on the low energy transitions.

for a 300 nm thick polycrystalline film deposited on a glass substrate.²⁹ The reduced mass is then used as a fixed parameter in the fitting of the excitonic transitions, which strongly constrains the value of the exciton binding energy, which must also be consistent with the 1s-2s separation observed at zero field. The zero field splitting follows the series of 3 dimensional hydrogen-like energy states

$$E_n = E_g - \frac{R^*}{n^2},$$

where E_n is the energy of the n^{th} excitonic level and $R^* = R_0\mu/m_0\varepsilon_r^2$, where R_0 is the atomic Rydberg, and ε_r is the relative dielectric constant of the material. The fitting allows us to conclude that R^* at 2 K is $R^* = 16 \pm 2$ meV. This value is significantly smaller than early estimates at low temperature based on magneto-optical measurements of only the 1s state^{5,14,15} or temperature dependent absorption measurements¹⁶ (37-50 meV), but agrees well with recent experimental results on thin films.^{17-20,29,31}

The early results depended entirely on the correct estimation of the dielectric constant, which was taken to be close to the high frequency value, on the assumption that a reduced dielectric screening occurs when the exciton binding energy is larger than the optical phonon energy.¹⁴ The phonon structure is however considerably more complex,¹⁸ and the observation of optical phonon modes with energies from 8 meV to 16 meV^{21,36} suggests enhanced dielectric screening and, consequently, a value intermediate between the static³⁷ and the high frequency^{35,38} dielectric constant should be used.¹⁷

The observation of higher exciton energy levels and Landau states enables us to measure the exciton binding energy without making any assumptions about the dielectric constant, which we can then deduce directly

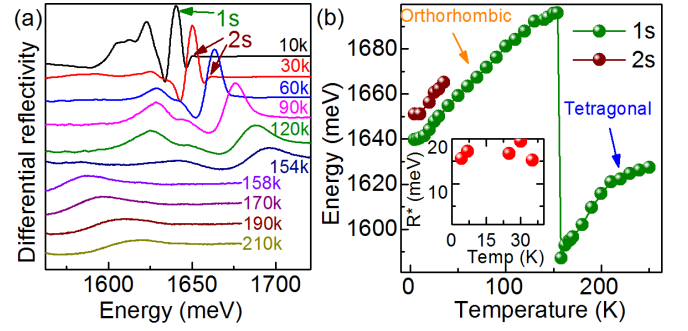


FIG. 3. (color online) (a) Differential reflectivity spectra measured at different temperatures. (b) 1s (green circles) and 2s (red circles) energy as a function of temperature. The inset indicates the exciton binding energy (estimated here from the 1s-2s splitting) as a function of the temperature.

from the above definition of the effective Rydberg to be $\varepsilon_r \sim 9.4$,²⁹ giving an effective exciton Bohr radius, a_B^* of 4.6 nm. The exciton binding energy obtained for the bulk MAPbI₃ crystal is thus identical, within experimental accuracy, to the binding energy of a randomly oriented polycrystalline film, determined with the same fitting procedure.²⁹ Our results imply that both the effective mass and the exciton binding energy are largely independent of the crystallinity and crystal orientation of the sample, as would be expected since the value of a_B^* is substantially larger than the size of the polycrystalline grains in typical device structures and the band structure is predicted to be essentially isotropic.^{34,35}

Practical device applications of perovskites, however, require a thorough understanding of the high temperature behavior of these materials, in particular in the high temperature tetragonal crystal phase which occurs above approximately 150 K.³⁹ The phase transition from orthorhombic to tetragonal is accompanied by a significant change of bandgap (~ 100 meV)^{16,17,19} as can be seen in Fig. 3(a) which shows differential reflectivity spectra at different temperatures. At zero magnetic field, we observe both 1s and 2s transitions at temperatures as high as 35 K, due to the excellent crystalline quality. The 1s and 2s peaks exhibit a similar blue shift with increasing temperature, as shown in Fig. 3(b), following the trend already observed for the 1s state in thin film samples.^{16,19,29} From 1s-2s separation we deduce R^* is independent of the temperature up to 35 K as shown in the inset in Fig. 3(b). Above 154 K there is an abrupt transition to a lower energy peak, red shifted by 103 meV with respect to the orthorhombic phase, which suggests that the entire area sampled by the excitation spot has completed the transition to the tetragonal phase.

We have repeated the magneto reflectivity measurements at 168 K and differential reflectivity spectra are shown in Fig. 4(a). The 1s state appears as a pronounced peak in the reflectivity spectrum even at low magnetic field, but with a considerable broadening (FWHM of 22 meV). A shallow peak related to the absorption of

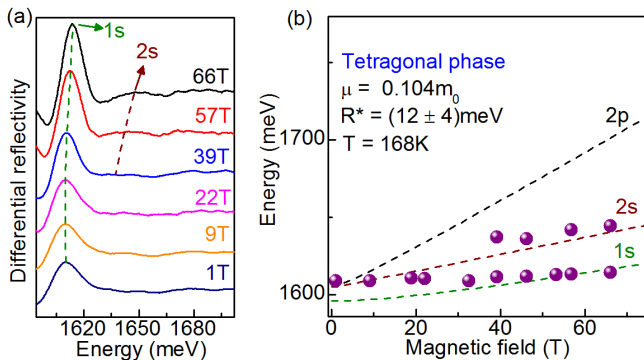


FIG. 4. (color online) (a) Magneto reflectivity spectra measured at $T = 168$ K differentiated with respect to energy. (b) High temperature energy fan chart. The dashed lines represent hydrogenic transitions.

the 2s state can be identified for magnetic fields larger than 39 T (Fig. 4(a)) but no higher energy transitions could be reliably identified. Figure 4(b) shows the transition energy fan chart at 168 K where the reduced mass has been assumed to be the same as at low temperature, $\mu \simeq 0.104m_0$. The exciton binding energy is expected to be more strongly affected by the phase transition. In the tetragonal phase, an increase of the dielectric constant is expected, due to the dynamic disorder related to the rotational motion of the organic cation enabled by the structural transition.⁴⁰ An increase of the dielectric screening should lead to a reduction of the exciton binding energy, with values reported for room temperature ranging from 5 to 12 meV.^{17,19,20}

We have fitted the data for the 1s and 2s transitions

above 30 T with the procedure described above and find an exciton binding energy of 12 ± 4 meV, comparable to that estimated by performing similar high temperature magneto transmission experiments on a thin film.²⁹ We consider this value to be an upper bound for the exciton binding energy at zero field, as the high frequency cyclotron motion in the high magnetic fields is expected to reduce the effective dielectric screening and hence increase the exciton binding energy.

In conclusion, we have studied the magneto optical properties of high quality single crystal MAPbI₃, which exhibits narrow 1s and 2s excitonic lines at low temperature and at zero magnetic field. Detailed magneto reflectivity measurements reveal that the exciton binding energy and effective masses are identical to those extracted from similar measurements on polycrystalline thin films deposited on glass substrates. The measured exciton binding energies, 16 meV for the low temperature orthorhombic phase and $\lesssim 12$ meV for the room temperature orthorhombic phase transition, are lower than the thermal energy at room temperature, consistent with organic-inorganic semiconducting perovskites showing non-excitonic behavior in solar cells and other devices.

ACKNOWLEDGMENTS

This work was partially supported by ANR JCJC project milliPICS, the Région Midi-Pyrénées under contract MESR 1305303, STCU project 5809 and the BLAPHENE project under IDEX program Emergence. This work was supported by EPSRC (UK) via its membership to the EMFL (grant no. EP/N01085X/1). ZY acknowledges financial support from the China Scholarship council. A.A.H acknowledges the support of the EPSRC Platform Grant (Grant No. EP/M020517/1).

* These authors contributed equally to the work

† paulina.plochocka@lncmi.cnrs.fr

‡ r.nicholas@physics.ox.ac.uk

¹ W. S. Yang, J. H. Noh, N. J. Jeon, Y. C. Kim, S. Ryu, J. Seo, and S. I. Seok, *Science* **348**, 1234 (2015).

² M. Saliba, T. Matsui, J.-Y. Seo, K. Domanski, J.-P. Correa-Baena, M. K. Nazeeruddin, S. M. Zakeeruddin, W. Tress, A. Abate, A. Hagfeldt, and M. Grätzel, *Energy & Environmental Science* **9**, 1989 (2016).

³ X. Li, D. Bi, C. Yi, J.-D. Décoppet, J. Luo, S. M. Zakeeruddin, A. Hagfeldt, and M. Grätzel, *Science*, aaf8060 (2016).

⁴ M. Saliba, T. Matsui, K. Domanski, J.-Y. Seo, A. Ummadisingu, S. M. Zakeeruddin, J.-P. Correa-Baena, W. R. Tress, A. Abate, A. Hagfeldt, and M. Grätzel, *Science* **354**, 206 (2016).

⁵ K. Tanaka, T. Takahashi, T. Ban, T. Kondo, K. Uchida, and N. Miura, *Solid State Communications* **127**, 619 (2003).

⁶ S. D. Stranks, G. E. Eperon, G. Grancini, C. Menelaou, M. J. P. Alcocer, T. Leijtens, L. M. Herz, A. Petrozza, and

H. J. Snaith, *Science* **342**, 341 (2013).

⁷ G. Xing, N. Mathews, S. Sun, S. S. Lim, Y. M. Lam, M. Grätzel, S. Mhaisalkar, and T. C. Sum, *Science* **342**, 344 (2013).

⁸ J. Burschka, N. Pellet, S.-J. Moon, R. Humphry-Baker, P. Gao, M. K. Nazeeruddin, and M. Grätzel, *Nature* **499**, 316 (2013).

⁹ M. Liu, M. B. Johnston, and H. J. Snaith, *Nature* **501**, 395 (2013).

¹⁰ Z.-K. Tan, R. S. Moghaddam, M. L. Lai, P. Docampo, R. Higler, F. Deschler, M. Price, A. Sadhanala, L. M. Pazos, D. Credgington, F. Hanusch, T. Bein, H. J. Snaith, and R. H. Friend, *Nature Nanotechnology* **9**, 687 (2014).

¹¹ H. Zhu, Y. Fu, F. Meng, X. Wu, Z. Gong, Q. Ding, M. V. Gustafsson, M. T. Trinh, S. Jin, and X. Y. Zhu, *Nature Materials* **14**, 636 (2015).

¹² Y. Fang, Q. Dong, Y. Shao, Y. Yuan, and J. Huang, *Nature Photonics* **9**, 679 (2015).

¹³ Y.-S. Park, S. Guo, N. S. Makarov, and V. I. Klimov, *ACS Nano* **9**, 10386 (2015).

¹⁴ M. Hirasawa, T. Ishihara, T. Goto, K. Uchida, and

- N. Miura, *Physica B: Condensed Matter* **201**, 427 (1994).
- ¹⁵ T. Ishihara, *Journal of Luminescence* **60**, 269 (1994).
- ¹⁶ V. D’Innocenzo, G. Grancini, M. J. P. Alcocer, A. R. S. Kandada, S. D. Stranks, M. M. Lee, G. Lanzani, H. J. Snaith, and A. Petrozza, *Nature Communications* **5**, 3586 (2014).
- ¹⁷ J. Even, L. Pedesseau, and C. Katan, *The Journal of Physical Chemistry C* **118**, 11566 (2014).
- ¹⁸ Q. Lin, A. Armin, R. C. R. Nagiri, P. Burn, and P. Meredith, *Nature Photonics* **9**, 106 (2015).
- ¹⁹ Y. Yamada, T. Nakamura, M. Endo, A. Wakamiya, and Y. Kanemitsu, *IEEE Journal of Photovoltaics* **5**, 401 (2015).
- ²⁰ A. M. Soufiani, F. Huang, P. Reece, R. Sheng, A. Ho-Baillie, and M. A. Green, *Applied Physics Letters* **107**, 231902 (2015).
- ²¹ L. Q. Phuong, Y. Nakaike, A. Wakamiya, and Y. Kanemitsu, *The Journal of Physical Chemistry Letters* **7**, 4905 (2016).
- ²² I. A. Shkrob and T. W. Marin, *The Journal of Physical Chemistry Letters* **5**, 1066 (2014).
- ²³ Z. Xiao, Q. Dong, C. Bi, Y. Shao, Y. Yuan, and J. Huang, *Advanced Materials* **26**, 6503 (2014).
- ²⁴ D. A. Valverde-Chávez, C. S. Ponseca, C. C. Stoumpos, A. Yartsev, M. G. Kanatzidis, V. Sundström, and D. G. Cooke, *Energy & Environmental Science* **8**, 3700 (2015).
- ²⁵ Q. Dong, Y. Fang, Y. Shao, P. Mulligan, J. Qiu, L. Cao, and J. Huang, *Science* **347**, 967 (2015).
- ²⁶ Z. Lian, Q. Yan, T. Gao, J. Ding, Q. Lv, C. Ning, Q. Li, and J.-l. Sun, *Journal of the American Chemical Society* **138**, 9409 (2016).
- ²⁷ J. Tilchin, D. N. Dirin, G. I. Maikov, A. Sashchiuk, M. V. Kovalenko, and E. Lifshitz, *ACS Nano* **10**, 6363 (2016).
- ²⁸ H.-H. Fang, R. Raissa, M. Abdu-Aguye, S. Adjokatse, G. R. Blake, J. Even, and M. A. Loi, *Advanced Functional Materials* **25**, 2378 (2015).
- ²⁹ A. Miyata, A. Mitioglu, P. Plochocka, O. Portugall, J. Tse-Wei Wang, S. D. Stranks, H. J. Snaith, and R. J. Nicholas, *Nature Physics* **11**, 582 (2015).
- ³⁰ K. P. Korona, A. Wyszomolek, K. Pakula, R. Stepniewski, J. M. Baranowski, I. Grzegory, B. Lucznik, M. Wroblewski, and S. Porowski, *Appl. Phys. Lett.* **69**, 788 (1996).
- ³¹ K. Galkowski, A. Mitioglu, A. Miyata, P. Plochocka, O. Portugall, G. E. Eperon, J. T.-W. Wang, T. Stergiopoulos, S. D. Stranks, H. J. Snaith, and R. J. Nicholas, *Energy & Environmental Science* **9**, 962 (2016).
- ³² P. C. Makado and N. C. McGill, *Journal of Physics C: Solid State Physics* **19**, 873 (1986).
- ³³ K. Watanabe, K. Ushida, and N. Miura, *Physical Review B* **68**, 155312 (2003).
- ³⁴ E. Menéndez-Proupin, P. Palacios, P. Wahnón, and J. C. Conesa, *Physical Review B* **90**, 045207 (2014).
- ³⁵ P. Umari, E. Mosconi, and F. De Angelis, *Scientific Reports* **4**, 4467 (2014).
- ³⁶ C. Quarti, G. Grancini, E. Mosconi, P. Bruno, J. M. Ball, M. M. Lee, H. J. Snaith, A. Petrozza, and F. De Angelis, *The Journal of Physical Chemistry Letters* **5**, 279 (2013).
- ³⁷ C. Wehrenfennig, M. Liu, H. Snaith, M. Johnston, and L. Herz, *Energy & Environmental Science* **7**, 2269 (2014).
- ³⁸ F. Brivio, K. Butler, A. Walsh, and M. van Schilfgaarde, *Physical Review B* **89**, 155204 (2014).
- ³⁹ T. Baikie, Y. Fang, J. M. Kadro, M. Schreyer, F. Wei, S. G. Mhaisalkar, M. Grätzel, and T. J. White, *Journal of Materials Chemistry A* **1**, 5628 (2013).
- ⁴⁰ A. Poglitsch and D. Weber, *The Journal of Chemical Physics* **87**, 6373 (1987).